Journal of the Optical Society of Korea
Vol. 20, No. 5, October 2016, pp. 601-606

ISSN: 1226-4776(Print) / ISSN: 2093-6885(Online)
DOI: http://dx.doi.org/10.3807/JOSK.2016.20.5.601

Calculating the Threshold Energy of the Pulsed Laser Sintering of Silver and Copper Nanoparticles

Changmin Lee and Jae W. Hahn*

Nano Photonics Laboratory, School of Mechanical Engineering, Yonsei University, 50 Yonsei-ro, Seodaemun-gu, Seoul 03722, Republic of Korea

(Received June 30, 2016 : revised September 12, 2016 : accepted September 12, 2016)

In this study, in order to analyze the low-temperature sintering process of silver and copper nanoparticles, we calculate their melting temperatures and surface melting temperatures with respect to particle size. For this calculation, we introduce the concept of mean-squared displacement of the atom proposed by Shi (1994). Using a parameter defined by the vibrational component of melting entropy, we readily obtained the surface and bulk melting temperatures of copper and silver nanoparticles. We also calculated the absorption cross-section of nanoparticles for variation in the wavelength of light. By using the calculated absorption cross-section of the nanoparticles at the melting temperature, we obtained the laser threshold energy for the sintering process with respect to particle size and wavelength of laser. We found that the absorption cross-section of silver nanoparticles has a resonant peak at a wavelength of close to 350 nm, yielding the lowest threshold energy. We calculated the intensity distribution around the nanoparticles using the finite-difference time-domain method and confirmed the resonant excitation of silver nanoparticles near the wavelength of the resonant peak.

Keywords : Laser sintering, Copper nanoparticle, Silver nanoparticle, Melting temperature, Threshold energy
OCIS codes : (160.4236) Nanomaterials; (160.3900) Metals; (350.4990) Particles; (120.4610) Optical fabrication

I. INTRODUCTION

Over the past few decades, techniques in printed electronics have emerged as an attractive alternative to the conventional manufacturing process [1-3]. These methods can help reduce the time and expense invested in conventional vacuum deposition and photolithographic patterning methods. Techniques using gold or silver nanoparticles have been proposed in the past because of their high conductivity and stability [4]. However, these noble metals are extremely costly in the context of commercialization. To solve this problem, many researchers have proposed alternative materials such as copper [3, 5, 6]. Copper is a suitable alternative to noble metals owing to its high conductivity and low cost.

Researchers have recently succeeded in printing electric circuits on plastic or organic substrates, which are sensitive to temperature. According to this trend, the low-temperature manufacturing process has been an important issue [7-10]. To solve this, various methods have been suggested. Some researchers have carried out low-temperature sintering by controlling pressure [11], whereas others have done so by using chemical reactions [12]. With regard to the sintering process, several researchers have also used size effects, whereby the melting temperature of a metallic particle decreases with size [13, 14]. Most relevant research has focused on experimental results. Therefore, there is considerable space for a theoretical approach in research on the sintering process.

There are three typical melting hypotheses concerning size effects [15, 16]. The first is the homogeneous melting hypothesis. In this case, the temperature is fixed for the entire melting process without the surface melting process. Using this hypothesis, the first model of the melting temperature function $T_m(r)$ was developed by Lindemann in 1910 [17]. He explained the melting transition by appealing to

*Corresponding author: jaewhahn@yonsei.ac.kr

Color versions of one or more of the figures in this paper are available online.

the vibrations of atoms in the crystal. However, this hypothesis is insufficient to explain the surface melting process occurring in the model.

The second hypothesis for the melting process is the liquid skin melting process [18]. In this process, a thin layer of liquid forms on the solid core at a low melting temperature, which is called the surface melting temperature. The layer persists until the particle completely melts at its melting temperature. In this case, the model predicts a faster variation than the linear variation in the melting temperature with size, unlike in other models [16].

The third hypothesis is the liquid nucleation and growth model [19, 20]. In this case, the liquid layer formed on the solid core grows with respect to the increase in temperature. The above three models predict a size-dependent melting temperature. However, none of these is related to the energetic state of the atom [15, 21].

Shi proposed a model in 1994 that explains the melting temperature using the mean-squared displacement of nanoparticles [21, 22]. This model considers not only melting enthalpy, but also the vibrational component because the free energy of the crystal-liquid interface also depends on it [22]. In this case, the vibrational component of melting entropy is needed to calculate the melting temperature instead of the surface energy, which is difficult to measure.

To predict the sintering process, the relation between the size of the particles and radiation is also important because radiation from laser changes the temperature of the particles. Researchers have found many cases confirming the relation between the size of nanoparticles and radiation [23-26]. Among the relevant studies, the Mie theory explains the interaction between particles and radiation through the phenomena of scattering, absorption, and extinction [23, 24].

In this paper, we report on the theoretical analysis of the sintering of copper and silver by using the size effects and optical properties of nanoparticles. Using Shi's model, we calculated the melting temperatures and the surface melting temperatures of these particles. We assumed that the surface of solid nanoparticles was melted by a pulsed laser. In this sintering process, we analyzed the necessary minimum laser energy according to particle size and the wavelength of the laser. The finite-difference time-domain (FDTD) simulation was performed to confirm the resonant peak wavelength of nanoparticles.

II. THEORY

Figure 1 shows a schematic diagram of the laser sintering process. In the figure, the sintering area is determined by the area occupied by the laser. To simplify the calculation of the energy needed for the sintering of nanoparticles, we used two assumptions. First, only one particle was irradiated in the area of the laser. Second, the sintering process is rapid enough for us to ignore energy loss due to conduction.

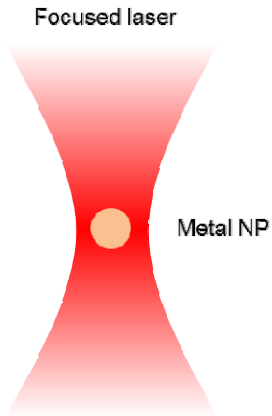

FIG. 1. Laser sintering process with metal nanoparticles.

Oxidation reaction can be ignored due to short sintering time less than 2ms [9]. The input laser power, which changes to heat energy, increases the temperature of particles. This process can be expressed as in Eq. (1):

$$C_p \rho_s V\left(T_f - T_i\right) = J\sigma(r,\lambda), \tag{1}$$

where C_p, ρ_s, V, T_f, T_i, $\sigma(r, \lambda)$, and J represent heat capacity, solid density, volume, final temperature, initial temperature, the absorption cross-section of the particle, and emitted energy of laser per unit area, respectively. According to Mie's theory, the absorption cross-section is defined as in Eq. (2) [23, 24]:

$$\sigma(r,\lambda) = 4\pi k r^3 \,\mathrm{Im}\left(\frac{\varepsilon-\varepsilon_m}{\varepsilon+2\varepsilon_m}\right), \tag{2}$$

where k, r, ε, and ε_m represent the propagation vector, the radius of the particle, the dielectric constant of metal, and the dielectric constant of the medium, respectively. In Eq. (1), the temperature change of copper is only determined by the energy of the illuminated laser.

In order to analyze the sintering process, we need to consider the melting temperature $T_m(r)$ function with respect to radius r. In Shi's model, the relation between melting temperature $T_m(\zeta)$ and bulk melting temperature $T_m(\infty)$ can be expressed as in Eq. (3) [20, 21]:

$$\frac{T_m(\zeta)}{T_m(\infty)} = \exp\left[-(\alpha-1)/(\zeta-1)\right]. \tag{3}$$

The parameter α is defined by the expression

$$\alpha = \frac{2S_{vib}(\infty)}{3R} + 1, \tag{4}$$

where S_{vib} and R are the vibrational component of melting entropy and the ideal gas constant, respectively. The

TABLE 1. Physical constants of copper and silver

Constant	Copper	Silver
Vibrational component of melting entropy S_{vib} (J/mol · K) [28]	8.06	7.98
Parameter α [28]	1.65	1.64
h (nm) [27]	0.2826	0.3194
Bulk melting temperature (K) [28]	1357.6	1234.93
Specific heat (J/kg·K) [29]	384.6	235.0
Density (kg/m^3) [29]	8.96×10^3	10.49×10^3

parameter ζ is defined as

$$\zeta = r/r_0. \tag{5}$$

Here, r and r_0 are the radius of the nanoparticle and the shape parameter. The shape parameter r_0 is given by $r_0 = (3-d)h$, where h is the atomic diameter. When the particle is a spherical nanoparticle, the dimension of the crystal d = 0 [21]. As mentioned above, the surface melting temperature also needs to be calculated for the threshold energy. The relation between the surface melting temperature $T_{sm}(\zeta)$ and bulk melting temperature $T_m(\infty)$ can be expressed as in Eq. (6):

$$\frac{T_{sm}(\zeta)}{T_m(\infty)} = (\alpha\eta_s)^{-1}\left\{1+\frac{\alpha-1}{\zeta-1}\right\}\exp\left[-\frac{\alpha-1}{\zeta-1}\right]. \tag{6}$$

In Eq. (6), the order parameter η_s = 0.75. This value is obtained from Landau's equation [21]. In the above equations, parameters ζ and α are always greater than 1 by definition. The surface melting temperature is the temperature at which the surface of a particle changes to a quasi- liquid surface layer [27]. Therefore, the surface temperature has to be smaller than the melting temperature if surface melting occurs. The detailed physical constants are listed in Table 1.

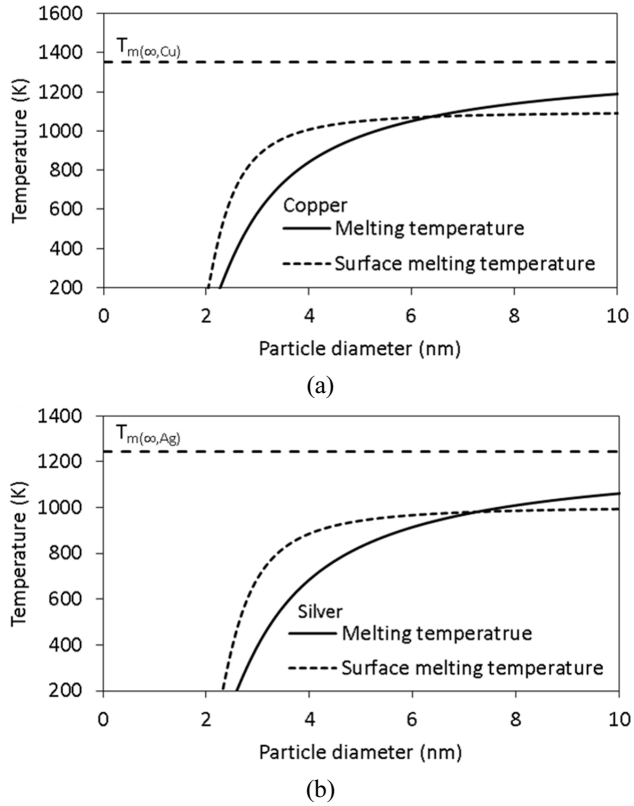

FIG. 2. Melting and surface melting temperatures for (a) copper and (b) silver nanoparticles.

III. RESULTS OF CALCULATION AND ANALYSIS

3.1. Melting Temperature and Surface Melting Temperature

From Eqs. (3) and (6), the melting and surface melting temperatures can be obtained. As shown in Fig. 2, the two have a positive relationship with the size of nanoparticles. Figure 2(a) shows the melting temperature and the surface melting temperature change for the size of copper. As the size decreased, the melting temperature decreased as well. Figure 2(b) shows the results for silver. The surface melting temperature was 300 K lower than the bulk melting temperature in the region greater than 6 nm in the case of copper. This difference can also be observed in the case of silver. In the region where the melting temperature was higher than the surface melting temperature, the particle began to melt at the surface melting temperature. At the surface melting temperature, only the surface of the particle had melted. Therefore, the surface melting temperature is also known as the pre-melting temperature. As mentioned in the introduction section, the layer of the quasi-liquid on the surface formed in that region. However, in the region where the surface melting temperature was higher than the melting temperature, the particle started to melt at the melting temperature without the occurrence of the surface melting process. The radius where the melting and surface melting temperature are the same is called the critical radius. In our results, the critical radii of copper and silver were 3.17 nm and 3.62 nm, respectively [28]. Using these results, we calculated the final temperature from Eq. (1). If particle

size was greater than the critical radius, the final temperature was identical to the surface melting temperature. However, if the particle size was smaller than the critical radius, the final temperature of the particle (T_f) was equal to the melting temperature.

3.2. Absorption Cross-section

Figure 3 shows the absorption cross-section spectra of copper and silver nanoparticles each with a 10-nm diameter. These results were obtained through Eq. (2). In the calculation, optical properties referred to previous researches [30, 31]. Eq. (2) states that the absorption cross-section is proportional to r^3 and k. Therefore, as wavelength increased, the absorption cross-section showed a tendency toward steady decline in the figure. However, the graph of copper, unlike silver, has no peak in the figure. This is due to the optical properties of copper [31]. However, the silver nanoparticle had a high peak value when the wavelength was close to 352 nm.

In order to check the results, we compared the results of the calculation for the absorption cross-section with the FDTD simulation of intensity distribution about the nanoparticle. The results of the FDTD simulation regarding the intensity distribution of nanoparticles are shown in Fig. 4(a)-(d). For the simulation, the polarized beam represented along the y-axis was used as the laser source. A perfect matched layer (PML) was used as the boundary condition. Figure 4(a) and (b) show the intensity distribution of a silver particle with a diameter of 10 nm at wavelengths of 355 nm and 532 nm, respectively. In Fig. 4(a), high intensity is observed around silver nano particle at wavelength of 355nm which is close to the peak of absorption cross section in Fig. 3. This peak represents the localized surface plasmon resonance (LSPR) peak of the silver nanoparticles [32]. LSPR is the collective electron charge oscillation in metallic nanoparticles excited by electromagnetic waves [33]. Figure 4(c) and (d) show the simulation results for intensity distribution of a copper particle with the same diameter of 10 nm at wavelengths of 355 nm and 532 nm, respectively. These results showed that the copper nanoparticle, illuminated by a wavelength of 355 nm, had higher intensity than in the 532 nm case.

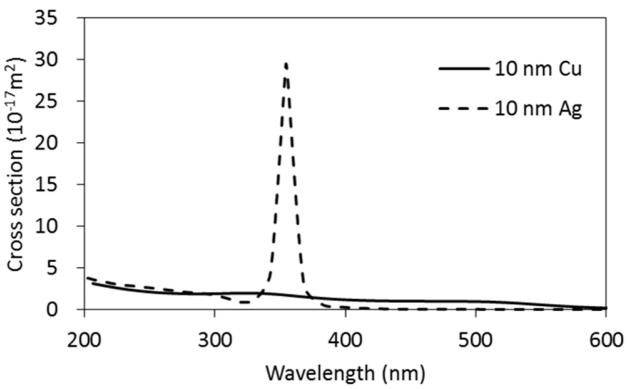

FIG. 3. Absorption cross-section of copper and silver nanoparticles with a diameter of 10 nm.

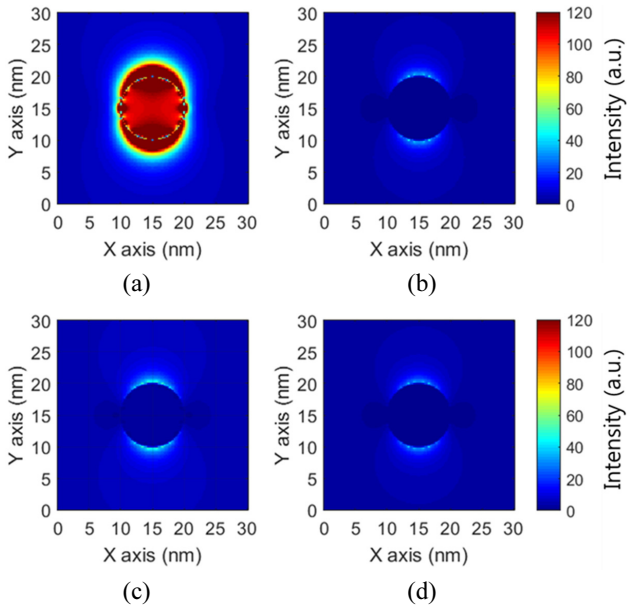

FIG. 4. FDTD simulation results for the intensity distribution of (a) silver nanoparticle at a wavelength of 355 nm, (b) silver nanoparticle at a wavelength of 532 nm, (c) copper nanoparticle at a wavelength of 355 nm, and (d) copper nanoparticle at a wavelength of 532 nm, each with a 10-nm diameter. The figures use bars of the same color to represent each particle.

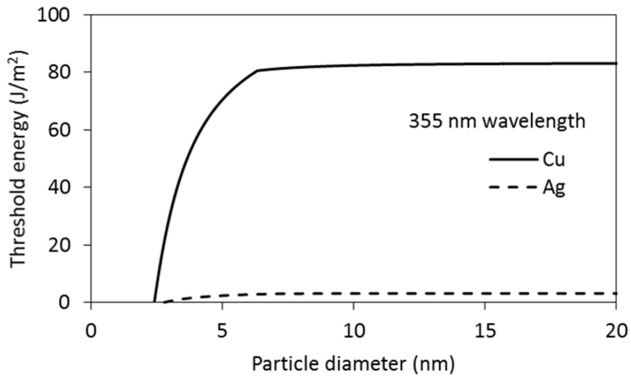

FIG. 5. Threshold energy with respect to the diameter of a particle at a wavelength of 355 nm.

These simulation results satisfactorily matched our calculated absorption cross-section results.

3.3. Threshold Energy

Figure 5 shows the threshold energy with respect to the diameter of copper and silver particles when the wavelength of the laser was 355 nm. The results were calculated using Eq. (1). The trend shown in Fig. 5 is similar to that evident in the graph of the melting temperature. The threshold energy of copper is greater than that of silver because of the absorption cross-section of the particle. As mentioned in Section 3.2,

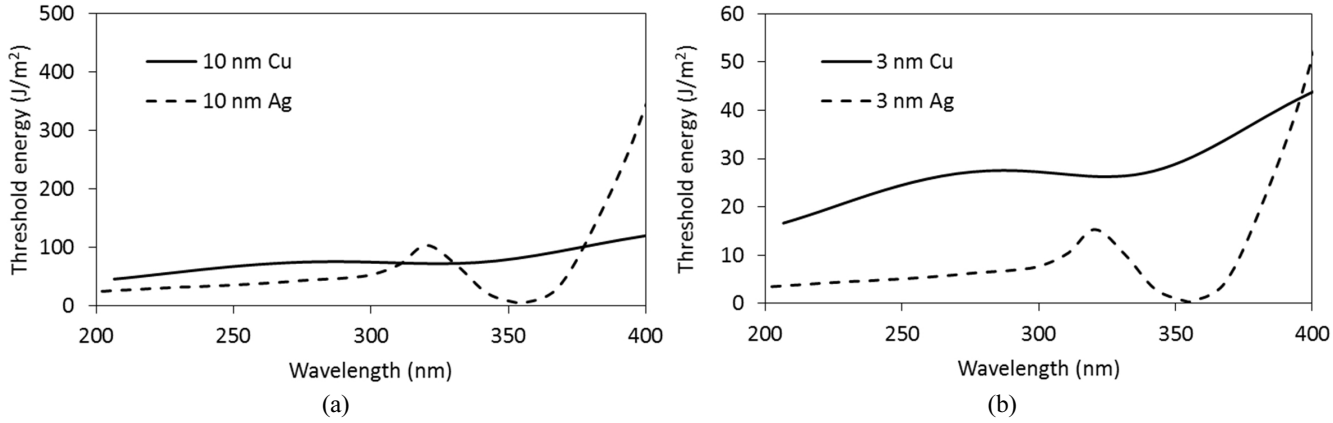

FIG. 6. Threshold energy versus wavelength of copper and silver particles with a (a) 10-nm and (b) 3-nm diameter.

the silver nanoparticle had peak absorption cross-section at a 352-nm wavelength. Due to the peak wavelength, the threshold energy of the silver was lower than that of copper. The threshold energy converged to 84 J/m^2 in the copper case and 3.2 J/m^2 in the silver case. In Fig. 5, the bending point was 6.34 nm in the case of copper. As mentioned in Section 3, half of 6.34 nm is the critical radius. Given this, we know that in the region where the diameter of the particle was smaller than the critical radius, the threshold energy was determined by the melting temperature, and by the surface melting temperature in other regions.

Figure 6(a) and (b) show the threshold energy according to the wavelength of the laser with particles of diameter 10 nm and 3 nm, respectively. In most regions, the threshold energy of copper was greater than that of silver. Whereas the threshold energy of copper increased slowly in most regions, that of silver reached its minimum value when the wavelength of the laser was 352 nm, and increased rapidly following that. This was due to the absorption cross-section spectrum. The threshold energy is inversely proportion to the absorption cross-section. Therefore, the threshold energy of copper, which has slow variation in absorption cross-section, increased slowly. However, the threshold energy of silver which, has high absorption cross-section at 352 nm, increased sharply beyond the peak wavelength.

IV. CONCLUSION

In this study, we proposed the minimum laser energy per unit area for the sintering of copper and silver nanoparticles through simple modeling. We calculated the melting temperature and the surface melting temperature of the copper and silver nanoparticles by using Shi's model. To find the threshold energy, we applied Mie theory to the energy balance equation. Our calculations showed that the wavelength was the major factor affecting the threshold energy in regions of short wavelength. In these regions, the threshold energy of silver was at its minimum value when the wavelength of the laser was 352 nm, which represents the wavelength of LSPR. However, in the case of copper, the minimum value was at the shortest wavelength in the calculated region. We also found that the peak of the absorption cross section well matched to a LSPR peak confirmed with FDTD simulation.

ACKNOWLEDGMENT

This work was supported by the National Research Foundation of Korea (NRF) grant funded by the Korea government (MSIP) (NRF-2015R1A2A1A03064460)

REFERENCES

1. J. Perelaer, B. de Gans, and U. S. Schubert, "Ink-jet printing and microwave sintering of conductive silver tracks," Adv. Mater. **18**, 2101-2104 (2006).
2. Q. Huang, W. Shen, Q. Xu, R. Tan, and W. Song, "Room-temperature sintering of conductive Ag films on paper," Mater. Lett. **123**, 124-127 (2014).
3. J. S. Kang, H. S. Kim, J. Ryu, H. T. Hahn, S. Jang, and J. W. Joung, "Inkjet printed electronics using copper nanoparticle ink," J. Mater. SCI-mater. EL. **21**, 1213-1220 (2010).
4. T. Kumpulainen, J. Pekkanen, J. Valkama, J. Laakso, R. Tuokko, and M. Mäntysalo, "Low temperature nanoparticle sintering with continuous wave and pulse lasers," Opt. Laser Technol. **43**, 570-576 (2011).
5. J. H. Yu1, K. T. Kang, J. Y. Hwang, S. H. Lee, and H. Kang, "Rapid sintering of copper nano ink using a laser in air," Int. J. Precis. Eng. Man. **15**, 1051-1054 (2014).
6. J. Lee, B. Lee, S. Jeong, Y. Kim, and M. Lee, "Enhanced surface coverage and conductivity of cu complex ink-coated films by laser sintering," Thin Solid Films **564**, 264-268 (2014).
7. J. Guo, H. Guo, A. L. Baker, M. l. T. Lanagan, E. R. Kupp, G. L. Messing, and C. A. Randall, "Cold sintering: A paradigm shift for processing and integration of ceramics,"

Angew. Chem. **128**, 11629-11633 (2016).
8. I. Shishkovsky, V. Scherbakof, and I. Volyansky, "Low-dose laser sintering of cu nanoparticles on the ceramic substrate during ink-jet interconnection," Proc. SPIE, 9065 (2014) 90650I-1-6.
9. H. S. Kim, S. R. Dhage, D. E. Shim, and H. T. Hahn, "Intense pulsed light sintering of copper nanoink for printed electronics," Appl. Phys. A **97**, 791-798 (2009).
10. H. Yu, L. He, M. Zeng, J. Liu, E. Li, X. Zhou, and S. Zhang, "Low temperature sintering of $Zn_{1.8}SiO_{3.8}$ dielectric ceramics containing $3ZnO\text{-}2B_2O_3$ glass," Mater. Lett. **179**, 150-153 (2016).
11. Z. Z. Zhang and G. Q. Lu, "Pressure-assisted low-temperature sintering of silver paste as an alternative die-attach solution to solder reflow," IEEE T. Electron. Pack. **25**, 279-283 (2002).
12. E. K. Yu, L. Piao, and S. H. Kim, "Sintering behavior of copper nanoparticles," B. Korean Chem. Soc. **32**, 4099-4102 (2011).
13. J. S. Kang, J. Ryu, H. S. KIM, and H. T. Hahn, "Sintering of inkjet-printed silver nanoparticles at room temperature using intense pulsed light," J. Electron. Mater. **40**, 2268-2277 (2011).
14. K. S. Moon, H. Dong, R. Maric, S. Pothukuchi, A. Hunt, Y. Li, and C. P. Wong, "Thermal behavior of silver nanoparticles for low-temperature interconnect applications," J. Electron. Mater. **34**, 168-175 (2005).
15. Z. Wen, M. Zhao, and Q. Jiang, "The melting temperature of molecular nanocrystals at the lower bound of the mesoscopic size range," J. Phys-Condens. Mat. **12**, 8819-8824 (2000).
16. K. K. Nanda, "Size-dependent melting of nanoparticles: Hundred years of thermodynamic model," Pramana − J. Phys. **72**, 617-628 (2009).
17. F. A. Lindemann, "Über die Berechnung molekularer Eigenfrequenzen," Physik. Z, **11**, 609-612 (1910).
18. C. R. M. Wronski, "The size dependence of the melting point of small particles of tin," Brit. J. Appl. Phys. **18**, 1731-1737 (1967).
19. P. R. Couchman and W. A. Jesser, "Thermodynamic theory of size dependence of melting temperature in metals," Nature **269**, 481-483 (1977).
20. S. C. Hendy, "A thermodynamic model for the melting of supported metal nanoparticles," Nanotechnology **18**, 175703-1-4 (2007).
21. Q. Jiang and C. C. Yang, "Size effect on the phase stability of nanostructures," Curr. Nanosci. **4**, 179-200 (2008).
22. Q. Jiang, H. X. Shi and M. Zhao, "Free energy of crystal-liquid interface," Acta Mater. **47**, 2109-2112 (1999).
23. S. A. Maier, *Plasmonics : fundamentals and applications*, (Springer, Bath, UK, 2007).
24. V. E. Ferry, J. N. Munday, and H. A. Atwater, "Design consideration for plasmonic photovoltaics," Adv. Mater. **22**, 4794-4808 (2010).
25. G. P. Wiederrecht, G. A. Wurtz, and J. Hranisavljevic, "Coherent coupling of molecular excitons to electronic polarizations of noble metal nanoparticles," Nano Lett. **4**, 2121-2125 (2004).
26. N. Guo, S. A. Dibenedetto, P. Tewari, M. T. Lanagan, M. A. Ratner, and T. J. Marks, "Nanoparticle, size, shape, and interfacial effects on leakage current density, permittivity, and breakdown strength of metal oxide-polyolefin nanocomposites: experiment and theory," Chem. Mater. **22**, 1567-1578 (2010).
27. A. P. Chernyshev, "Melting of surface layers of nanoparticles: Landau model," Mater. Chem. Phys. **112**, 226-229 (2008).
28. A. P. Chernyshev, "Effect of nanoparticle size on the onset temperature of surface melting," Mater. Lett. **63**, 1525-1527 (2009).
29. F. P. Incropera, D. P. DeWitt, T. L. Bergaman, and A. S. Lavine, *Introduction to heat transfer Fifth Ed.* (John Wiley & Sons, USA, 2007).
30. P. B. Johnson and R. W. Christy, "Optical constants of the noble metals," Phys. Rev. B **6**, 4370-4379 (1972).
31. A. D. Rakić, A. B. Djurišić, J. M. Elazar, and M. L. Majewski, "Optical properties of metallic films for vertical-cavity optoelectronic devices," Appl. Optics **37**, 5271-5283 (1998).
32. M. D. Malinsky, K. L. Kelly, G. C. Schatz, and R. P. Van Duyne, "Nanosphere lithography: effect of substrate on the localized surface plasmon resonance spectrum of silver nanoparticles," J. Phys. Chem. B **105**, 2343-2350 (2001).
33. K. M. Byun, "Development of nanostructured plasmonic substrates for enhanced optical biosensing," J. Opt. Soc. Korea **14**, 65-76 (2010).